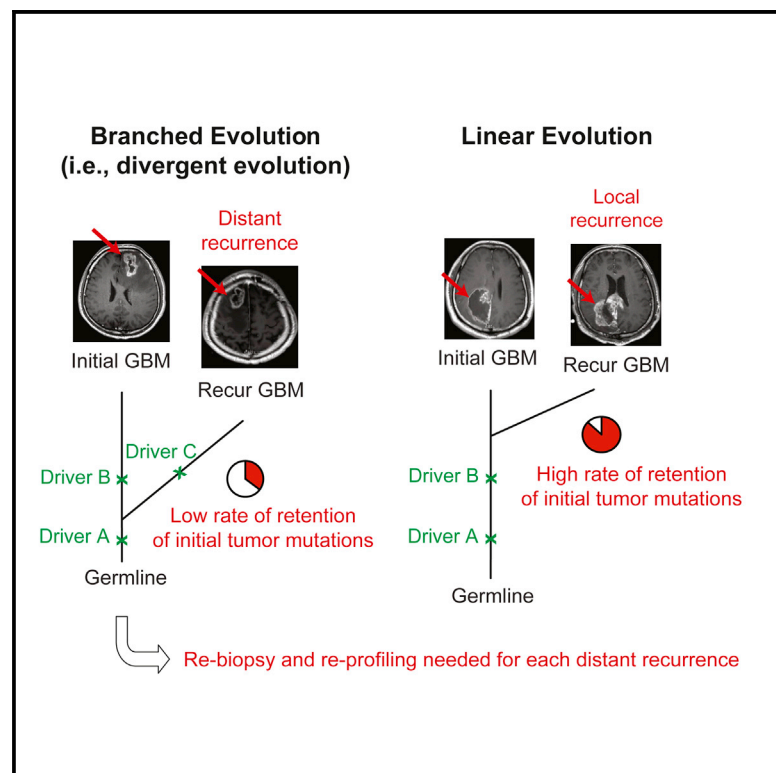


# Cancer Cell

## Spatiotemporal Evolution of the Primary Glioblastoma Genome

### Graphical Abstract



### Authors

Jinkuk Kim, In-Hee Lee, Hee Jin Cho, ..., Jeongwu Lee, Peter J. Park, Do-Hyun Nam

### Correspondence

[peter\\_park@harvard.edu](mailto:peter_park@harvard.edu) (P.J.P.), [nsmam@skku.edu](mailto:nsmam@skku.edu) (D.-H.N.)

### In Brief

Kim et al. find that glioblastomas recurring at distant sites have driver genetic alterations very different from those of matched initial tumors. They also show that, in contrast to *IDH1*-mutated tumors, *IDH1*-wild-type primary glioblastomas rarely develop hypermutation following temozolomide treatment.

### Highlights

- Distant recurrence predicts branched evolution of the paired tumors
- Distant recurrence frequently involves divergence in key GBM driver alterations
- Recurrent GBMs have more aberrations in core GBM driver pathways than initial GBMs
- TMZ-induced hypermutation is rare in *IDH1*-wild-type primary GBMs

### Accession Numbers

GSE63035



# Spatiotemporal Evolution of the Primary Glioblastoma Genome

Jinkuk Kim,<sup>1,3,12</sup> In-Hee Lee,<sup>1,2,12</sup> Hee Jin Cho,<sup>1,4,12</sup> Chul-Keek Park,<sup>5,12</sup> Yang-Soon Jung,<sup>6</sup> Yanghee Kim,<sup>1</sup> So Hee Nam,<sup>1</sup> Byung Sup Kim,<sup>6</sup> Mark D. Johnson,<sup>8</sup> Doo-Sik Kong,<sup>6</sup> Ho Jun Seol,<sup>6</sup> Jung-Il Lee,<sup>6</sup> Kyeong Min Joo,<sup>1,4,7</sup> Yeup Yoon,<sup>1,4</sup> Woong-Yang Park,<sup>1,2,4</sup> Jeongwu Lee,<sup>11</sup> Peter J. Park,<sup>9,10,13,\*</sup> and Do-Hyun Nam<sup>1,4,6,13,\*</sup>

<sup>1</sup>Samsung Biomedical Research Institute

<sup>2</sup>Samsung Genome Institute

Samsung Medical Center, Seoul 06351, Korea

<sup>3</sup>Samsung Advanced Institute of Technology, Samsung Electronics Co., Ltd., Seoul 06351, Korea

<sup>4</sup>Department of Health Sciences and Technology, Samsung Advanced Institute for Health Science and Technology (SAIHST), Sungkyunkwan University, Seoul 06351, Korea

<sup>5</sup>Department of Neurosurgery, Seoul National University Hospital, Seoul National University College of Medicine, Seoul 06351, Korea

<sup>6</sup>Department of Neurosurgery, Samsung Medical Center

<sup>7</sup>Department of Anatomy and Cell Biology

Sungkyunkwan University School of Medicine, Seoul 06351, Korea

<sup>8</sup>Department of Neurosurgery

<sup>9</sup>Division of Genetics

Brigham and Women's Hospital, Boston, MA 02115, USA

<sup>10</sup>Department of Biomedical Informatics, Harvard Medical School, Boston, MA 02115, USA

<sup>11</sup>Department of Stem Cell Biology and Regenerative Medicine, Lerner Research Institute, Cleveland Clinic, Cleveland, OH 44195, USA

<sup>12</sup>Co-first author

<sup>13</sup>Co-senior author

\*Correspondence: [peter\\_park@harvard.edu](mailto:peter_park@harvard.edu) (P.J.P.), [nsham@skku.edu](mailto:nsham@skku.edu) (D.-H.N.)

<http://dx.doi.org/10.1016/j.ccell.2015.07.013>

## SUMMARY

Tumor recurrence following treatment is the major cause of mortality for glioblastoma multiforme (GBM) patients. Thus, insights on the evolutionary process at recurrence are critical for improved patient care. Here, we describe our genomic analyses of the initial and recurrent tumor specimens from each of 38 GBM patients. A substantial divergence in the landscape of driver alterations was associated with distant appearance of a recurrent tumor from the initial tumor, suggesting that the genomic profile of the initial tumor can mislead targeted therapies for the distally recurred tumor. In addition, in contrast to *IDH1*-mutated gliomas, *IDH1*-wild-type primary GBMs rarely developed hypermutation following temozolomide (TMZ) treatment, indicating low risk for TMZ-induced hypermutation for these tumors under the standard regimen.

## INTRODUCTION

Glioblastoma multiforme (GBM; World Health Organization grade IV glioma) is the most common and most aggressive brain tumor (Furnari et al., 2007; Tanaka et al., 2013). GBMs can be classified into two categories, on the basis of the history of tumor

onset. More than 90% of GBMs present as de novo GBMs (primary GBMs), and the remainder progress from low-grade (grades I–III) gliomas (secondary GBMs). The current therapeutics for GBM serve mostly as palliative measures. Despite aggressive treatment with surgery, radiation, and the alkylating agent temozolomide (TMZ), GBM almost always recurs, and

### Significance

Although previous sequencing studies examined the genomic landscape of GBMs and their evolution, they did not relate genomic evolution patterns to tumor location or treatment regimens. Our integrative clinical and genomic analyses of 38 longitudinal pairs reveal that a recurrent tumor at a distant brain site from the initial tumor has a highly divergent genomic profile compared with the initial tumor, suggesting that the location of recurrence should be considered when using the genomic profile of the initial tumor to guide targeted therapies for the recurrent tumor. Our study also demonstrates that *IDH1*-wild-type primary GBMs have low risk for TMZ-induced hypermutation following the standard regimen. These findings provide critical insights for informed clinical decisions.

the median survival of GBM patients is only 15 months (Stupp et al., 2005).

Great strides have been made in understanding the genomic architecture of GBM. The Cancer Genome Atlas (TCGA) (Brennan et al., 2013; Cancer Genome Atlas Research Network, 2008) and other genomic studies of GBM have identified several core oncogenic pathways, such as p53, Rb, and receptor tyrosine kinase (RTK)/Ras/phosphoinositide 3-kinase (PI3K) signaling (Cancer Genome Atlas Research Network, 2008), as well as *MGMT* (Esteller et al., 2000), *IDH1* (Parsons et al., 2008; Yan et al., 2009), *TERT* (Killela et al., 2013), and chromatin modifier genes such as *H3F3A* and *ATRX* (Jiao et al., 2012; Schwartzentruber et al., 2012; Sturm et al., 2012; Wu et al., 2012a). Transcriptional profiling has shown that GBMs can be stratified into four or five molecular subtypes (Noussimh et al., 2010; Verhaak et al., 2010). In addition, a genomic study on longitudinal pairs of GBMs (Kim et al., 2015) described the patterns of genomic evolution at recurrence. However, because of the unavailability of the full clinical data, including magnetic resonance (MR) images and treatment dosages for each patient, the study provided limited insights into the clinical relevance of the genomic evolution patterns.

In contrast to other solid tumors, glioma cells do not depend on intravascular or lymphatic routes to spread (Cuddapah et al., 2014). Instead, glioma cells migrate mainly through perivascular space and the brain parenchyma. Accordingly, although metastasis into extracranial tissues is uncommon, GBM cells are highly invasive and infiltrative in the brain. Hence, GBMs recur not only at the sites of the initial tumors (local recurrence) but also commonly at different anatomical sites of the brain (distant recurrence), including in the other hemisphere relative to the initial tumor site. Although this pattern of tumor recurrence has been recognized in the clinic, few, if any, studies have examined the evolutionary processes leading to local versus distant recurrence.

Another important question about the recurrence of primary GBMs concerns the type and extent of the genomic damage inflicted by TMZ treatment. TMZ is a potent DNA-damaging agent that alkylates guanine residues (Stevens and Newlands, 1993). Although mutagenic effects of TMZ are well recognized (Bodell et al., 2003), its therapeutic benefit in extending GBM patients' survival has been demonstrated in large cohort studies (Stupp et al., 2005, 2007). In a recent study by Johnson et al. (2014), tumor genome evolution from *IDH1* mutation-harboring low-grade gliomas to higher grade malignancies was examined by sequencing in 23 patients. The authors observed that in 6 of the 10 TMZ-treated glioma patients, the recurrent tumors displayed TMZ-associated hypermutation—a massive accumulation of mutations known to be induced by TMZ treatment (C-to-T transition in CpC and CpT contexts)—and the same tumors displayed more oncogenic aberrations and progression to grade IV at recurrence. These findings were taken to imply that TMZ treatment might have side effects for patients with low-grade gliomas. Because TMZ is part of the standard of care for GBM patients, a very important issue is whether TMZ-associated hypermutation is frequent also in primary GBMs. Incidents of hypermutation had been reported in GBM tumors from patients who were previously treated with alkylating agents including TMZ and CCNU (lomustine) (Cahill et al., 2007; Cancer

Genome Atlas Research Network, 2008; Hunter et al., 2006; Kim et al., 2015; Yip et al., 2009). However, solid conclusions had not been drawn, because of the limited number of tumors analyzed and the lack of sufficient clinical and genomic information, such as the dose and duration of TMZ treatment and *IDH1/2* mutation status. A better understanding of the mutagenic characteristics of TMZ will help in weighing the beneficial and adverse effects of TMZ for maximal clinical benefit.

## RESULTS

### Paired GBM Tumor Specimens from 38 Patients

We obtained paired longitudinal specimens from each of the 38 GBM patients (34 primary and 4 secondary GBM patients; Figures S1A and S1B and Table S1). Treatment-naïve initial tumors were available for 35 cases; for the other 3 cases (01, 04, and 07; all 3 were secondary GBM cases), we used the first recurrent tumors in lieu of initial tumors. These first recurrent tumors were naïve to TMZ and radiation treatment, except for case 07, whose first recurrent tumor was previously treated with radiation (Figure S1B). All 38 patients received both TMZ and radiation treatment between the surgical procedures during which specimens were obtained, except for case 07, who was treated only with TMZ between the procedures. Tumor specimens were subjected to whole-exome sequencing (WES; 27 cases at the median depth of 74X; WES for the matched normal was done for 22 of the 27 cases at the median depth of 68X), RNA sequencing (RNA-seq; 30 cases), and array-comparative genomic hybridization (aCGH; 16 cases).

### Substantial Genomic Divergence at Distant Recurrence

To determine the extent of genomic divergence between the initial and recurrent tumors, we first identified somatic mutations in each tumor and compared the mutation profiles between the initial and recurrent tumors in each case. For this analysis, we used 22 cases for which WES data were available for both the tumor and matched normal tissues, as the somatic origins of mutations can be unambiguously determined for these cases (Figure S1C). Mutation calling was done using MuTect, a widely used program (Cibulskis et al., 2013). To validate the mutation calls, we used two independent approaches. First, we performed Sanger sequencing for a subset of mutations, with mutant allele fraction (MAF) as low as 0.07 and read depth as low as 11 (Figure S1D and Table S2). Eighty-five percent (22 of 26) of tested mutation calls were validated, even though only a trace amount of genomic DNA was used for some reactions because of the low quantity of available material, and different specimens of the same tumors had to be used in some cases because of the unavailability of the original DNA samples. Second, we systematically compared WES mutation calls with those from the corresponding RNA-seq data sets. For this analysis, DNA and RNA were simultaneously prepared from the same piece of a tumor specimen. When subjecting WES mutation calls whose locus is expressed (covered by four or more reads in RNA-seq data), more than 92% of the WES mutation calls with read depth  $\geq 20$  and MAF  $\geq 0.2$  were confirmed in the corresponding RNA-seq data (Figure S1E). Together, these results support high accuracy of our WES mutation calls.

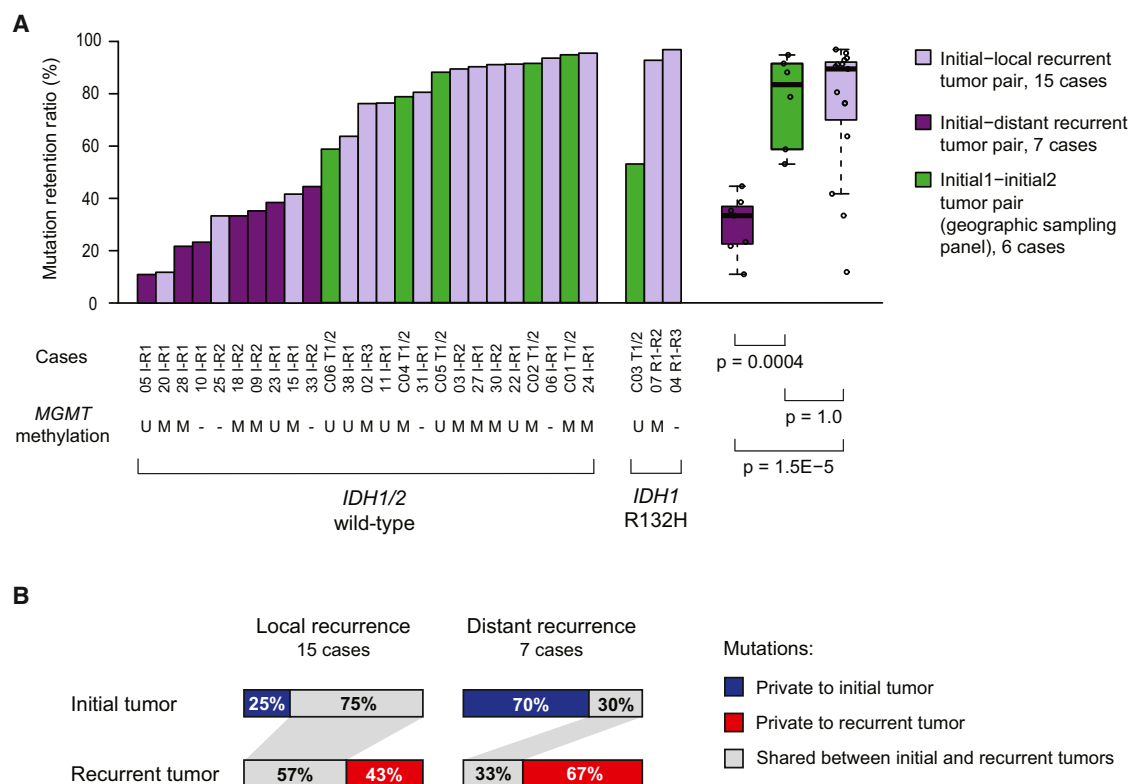


### Figure 1. Substantial Genomic Divergence at Distant Recurrence

(A) Mutation retention ratio and its relationship to the location of recurrence. For the longitudinal sampling panel (initial-recurrent tumor pairs; indicated with light and dark purple for local and distant recurrence cases, respectively), mutation retention ratio is defined as the percentage of mutations from the first available tumor retained in the last available recurrent tumor. For the geographic sampling panel (two geographically separated specimens of a common initial tumor; indicated with green), mutation retention ratio is the average of the two possible ratios. For box plots, the line inside the box is the median; the top and bottom of the box are the first and third quartiles, respectively; the lines above and below the box represent  $1.5 \times$  interquartile range above and below the median, respectively; and the dots mark individual data points. For p values, t tests were used. Somatic mutations (MAF  $\geq 0.2$  and read depth  $\geq 20$ ) in the 22 cases with WES data available for both the tumor and normal tissues were considered. Case labels (shown below the bar plot): I, initial tumor; R, recurrent tumor. *MGMT* promoter methylation status: M, methylated; U, unmethylated.

(B) The average fractions of shared and private mutations in the initial and recurrent tumors. Mutations considered for this analysis are as in (A). See also Figure S1 and Tables S1, S2, S3, and S4.

In addition, we conducted ultra-deep sequencing for four tumor specimens to exclude the possibility that the depth of our WES (74X) was not sufficient for the reliable detection of low-frequency mutations; frequent failures in the detection of low-frequency mutations may lead to misclassification of many shared mutations into private mutations, overestimating the number of private mutations. Our results strongly argue against that possibility: among the 17 private mutations tested by ultra-deep sequencing (minimum depth, 200X; mean depth, 1,001X), almost all (94% [16 of 17]) were confirmed to be absent from the tumor in which the mutations were originally undetected by WES (Figure S1F). Examination of an additional pair of tumors with the standard WES and ultra-deep sequencing also confirmed that all of the 29 mutations called as private by WES were indeed highly likely to be private (Figure S1G).

Having validated somatic mutations by multiple approaches, we determined the fraction of initial tumor mutations that were preserved in the recurrent tumors (mutation retention ratio) in each pair. Mutation retention ratios of the 22 cases varied widely from 11% to 97%, with two noticeable clusters near  $\sim 30\%$  and

$\sim 80\%$  (Figure 1A); this bimodal distribution of mutation retention levels was also reported in recent studies on paired gliomas (Johnson et al., 2014) and GBMs (Kim et al., 2015). Because a low mutation retention ratio is an indicator of branched evolution and substantial genomic divergence of the recurrent tumor from the initial tumor, we hypothesized that tumors with low retention ratios might be associated with specific clinical, biological, or genomic parameters (e.g., age, sex, radiographic tumor location, transcriptome subtype, *MGMT* promoter methylation, driver alterations). Statistical analysis showed no significant correlation of the mutation retention ratio with any of these parameters after multiple hypotheses correction, except for one: low mutation retention ratio was significantly correlated with distant recurrence ( $p = 0.003$ , Pearson correlation test, Bonferroni-corrected; Table S3). All 7 distant recurrent tumors retained fewer than half of the initial tumor mutations (25% on average). In contrast, 12 of 15 local recurrent tumors showed  $>50\%$  mutation retention (70% on average) (Figures 1A and 1B). This difference was highly significant by all other statistical tests applied ( $p < 0.002$  by t test, Wilcoxon test, and Kolmogorov-Smirnov test),

demonstrating that distally recurred tumors were highly divergent from the initial tumors, unlike locally recurred tumors.

Intratumoral heterogeneity has been well recognized in GBM (Holland, 2000), and recent studies using multi-region sequencing (Johnson et al., 2014; Sottoriva et al., 2013), fluorescence in situ hybridization (Snuderl et al., 2011), and single-cell sequencing (Francis et al., 2014; Nathanson et al., 2014; Patel et al., 2014) have collectively provided a more detailed characterization of this heterogeneity. To confirm that the genomic divergence of distant recurrent tumors observed above was not due to intratumoral heterogeneity, we collected and profiled two specimens from each of six new GBM cases (all with the matched normal) and assessed their degree of genomic divergence. In this “geographic sampling panel” (Table S4), two distinct specimens were sampled from a common untreated tumor of each patient (i.e., multi-region sequencing). To obtain an upper bound for intratumoral heterogeneity, we sampled phenotypically distinct specimens, with “phenotype” measured by (1) positive versus negative staining by a tumor-visualizing fluorescent dye, 5-aminolevulinic acid (Gliolan) (Sottoriva et al., 2013), (2) infiltrating edge versus central mass lesions, or (3) lobal versus ventricle-invading lesions (Figure S1H). In this geographic sampling panel, mutation retention ratios from the six cases (83% on average) were higher than the levels in the local recurrences (70% on average) and far higher than the levels in the distant recurrences (25% on average) ( $p = 0.001$ , Wilcoxon test) (Figure 1A). These data suggest that although intratumoral geographic heterogeneity does exist in GBMs, it cannot account for the striking genomic divergence in distant recurrence.

### Tumor Evolution in the Cases with Three Longitudinal Specimens

Analysis of multiple longitudinal samples can potentially provide a more comprehensive view on the spatiotemporal evolution of GBMs. Although multiple surgical resections after the initial surgery are very rare for primary GBM patients, we were able to obtain such specimens from four patients. We examined clinical history and genomic evolution in detail for each of these cases. For case 02 (Figure 2A), MR images showed that both resected recurrent tumors (R2 and R3) were at the same anatomical location as the initial tumor, which suggested that both the recurrent tumors likely retained a majority of the initial tumor mutations. This prediction was confirmed by our genomic analysis, which showed that the common ancestor clone of both recurrent tumors retained 76% (115 of 151, indicated by pie charts in Figure 2A) of the initial tumor mutations. For cases 09 and 18 (Figures 2B and 2C), two resected recurrent tumors were at a different anatomical location from the initial tumor in each case, making it likely that only a minor portion of the initial tumor mutations were retained in the recurrent tumors. Indeed, our genomic analysis showed that the common ancestor clone of the two recurrent tumors of each case retained fewer than half—35% (31 of 88) for case 09 and 33% (45 of 135) for case 18—of the initial tumor mutations. For case 09, we note that despite the large number of private mutations (125), R3 retained a majority of R1 mutations (68 of 111 [61%]), indicating that R3 had locally arisen from R1. For case 33 (Figure 2D), the first recurrent tumor was local and the second recurrent tumor was distal from the initial tumor. Our genomic analysis confirmed

that the first recurrent tumor retained 87% (88 of 101) of the mutations from the initial tumor, whereas the second recurrent tumor retained only 45% (45 of 101). Together, these four cases further illustrate that a distant location of a recurrent tumor is a strong indicator of a low level of mutation carry-over from the initial tumor to the recurrent tumor—hence, branched evolution and substantial divergence of the tumors.

### Divergence in Key GBM Driver Gene Alterations

To determine whether the substantial divergence in the overall mutational profile at distant recurrence entails changes in key GBM-driving events, we examined our tumor pairs for the alterations (including point mutations, structural variants, and copy number changes) that are frequently found in the TCGA GBMs (Brennan et al., 2013; Cancer Genome Atlas Research Network, 2008). Among these, the most prominent alterations in our cohort were deletions of *CDKN2A/B* and *PTEN*, inactivating mutations in *TP53* and *PTEN*, and activating mutations, structural variants, or amplification of *EGFR*. These alterations were detected in three or more cases of both local and distant recurrence groups (Figures 3A and S2A). We found that these GBM driver alterations were more frequently present as private events in distant recurrence cases (13 of 23 [57%]) than in local recurrence cases (7 of 35 [20%]) ( $p = 0.006$ , Fisher’s exact test). For instance, *TP53* mutations were private in only 1 of 6 local recurrence cases, whereas they were private in all 4 distant recurrence cases ( $p = 0.02$ ). *PTEN* mutations showed the similar trend (private in 0 of 3 and 3 of 4 in local and distant recurrence cases, respectively). Together, these results suggest that, in comparison with the initial tumors, distant recurrence entails more divergence in alterations of core driver genes than local recurrence.

### Convergent Evolution of the Paired Tumors

Through our paired analysis, we found evidence for convergent evolution, that is, independent clonal evolution to acquire different genomic alterations in the same gene (Figures 3A and 3B). For example, in the initial tumor of case 20, two mutations of *EGFR*—variant III (Batra et al., 1995; Sugawa et al., 1990) and A1148T—were detected at MAFs of 0.49 (73 of 148) and 0.12 (496 of 4,282), respectively. In the matched recurrent tumor, however, the above mutations were not detected; instead, an activating *EGFR* mutation G598V (Lee et al., 2006) was detected at an MAF of 0.19 (123 of 642). Similarly, while the initial tumor of case 10 harbored a *TP53* mutation A161T (MAF = 0.27; 27 of 100) in its DNA-binding domain, its recurrent tumor contained a different *TP53* mutation in the same domain, A138V (MAF = 0.48; 43 of 90). In addition, in case 18, potentially functional *PTEN*, *RB1*, and *NF1* mutations in the initial tumor were switched to different mutations of the same type in all three genes in the recurrent tumors (Figures 2C and 3B).

Evidence of convergent evolution was also found at the pathway level. The *CDKN2A/B* locus encodes INK4 and ARF proteins, which are central negative regulators of INK4-Rb and ARF-p53 pathways, respectively. In case 09, the initial tumor harbored *RB1* heterozygous deletion (for INK4-Rb pathway) in addition to *TP53* R158H mutation (MAF = 0.48 [11 of 23]; for ARF-p53 pathway) (Figures 2B, 3B, 3C, and S2B). These genes encode components of INK4-Rb and ARF-p53 pathways (Furnari et al., 2007). In contrast, the last recurrent tumor (R3) of

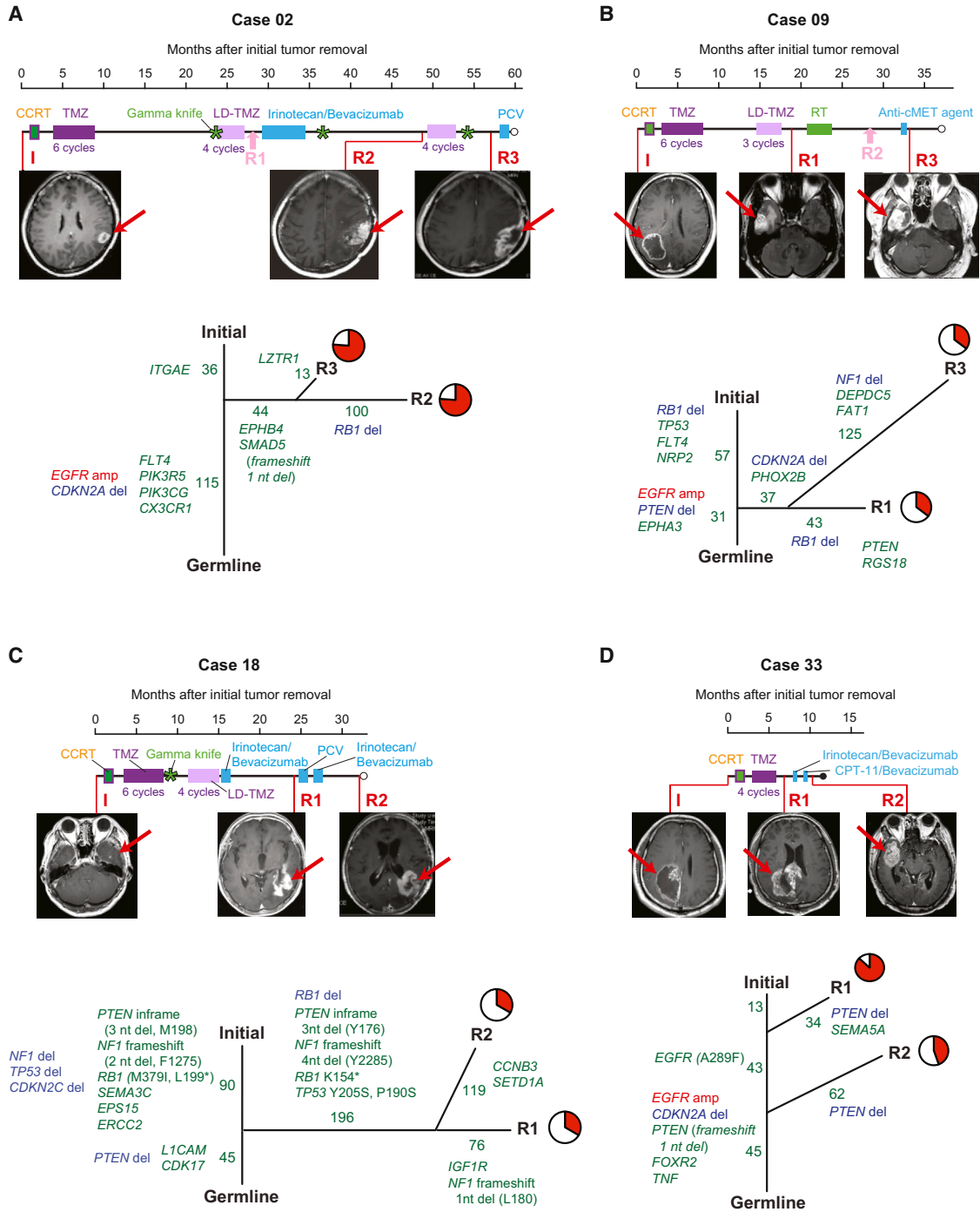


**Figure 2. Spatiotemporal Tumor Evolution in Four Patients**

(A–D) Treatment histories and tumor phylogenies for case 02 (A), case 09 (B), case 18 (C), and case 33 (D) with three longitudinal tumor specimens: the initial (I) and two recurrent (R) tumors each. LD-TMZ, low-dose TMZ; RT, radiation therapy; CCRT, concurrent chemoradiotherapy. MR images are preoperative; red arrows indicate the tumor tissues that were resected. On time lines, pink arrows indicate the times of surgical procedures from which no specimen was collected, hollow circles indicate the last follow-up, and solid circles indicate patient death. The phylogenetic trees below MR images illustrate the evolutionary relationship among the three tumors of each case. For each branch, the number of somatic point mutations and indels ( $MAF \geq 0.2$  and read depth  $\geq 20$ ) and the names of select mutated cancer genes that are attributed to the branch are shown. The length of a branch is proportional to the number of point mutations. Labeled in red and blue are focal, high-amplitude amplification ( $\geq 1.5$ ,  $\log_2$  scale) and heterozygous/homozygous deletion ( $\leq -0.5$ ), respectively. Labeled in green are genes with point mutations or indels. Pie charts next to recurrent tumor labels indicate the fraction of initial tumor mutations that are found in the recurrent tumor.

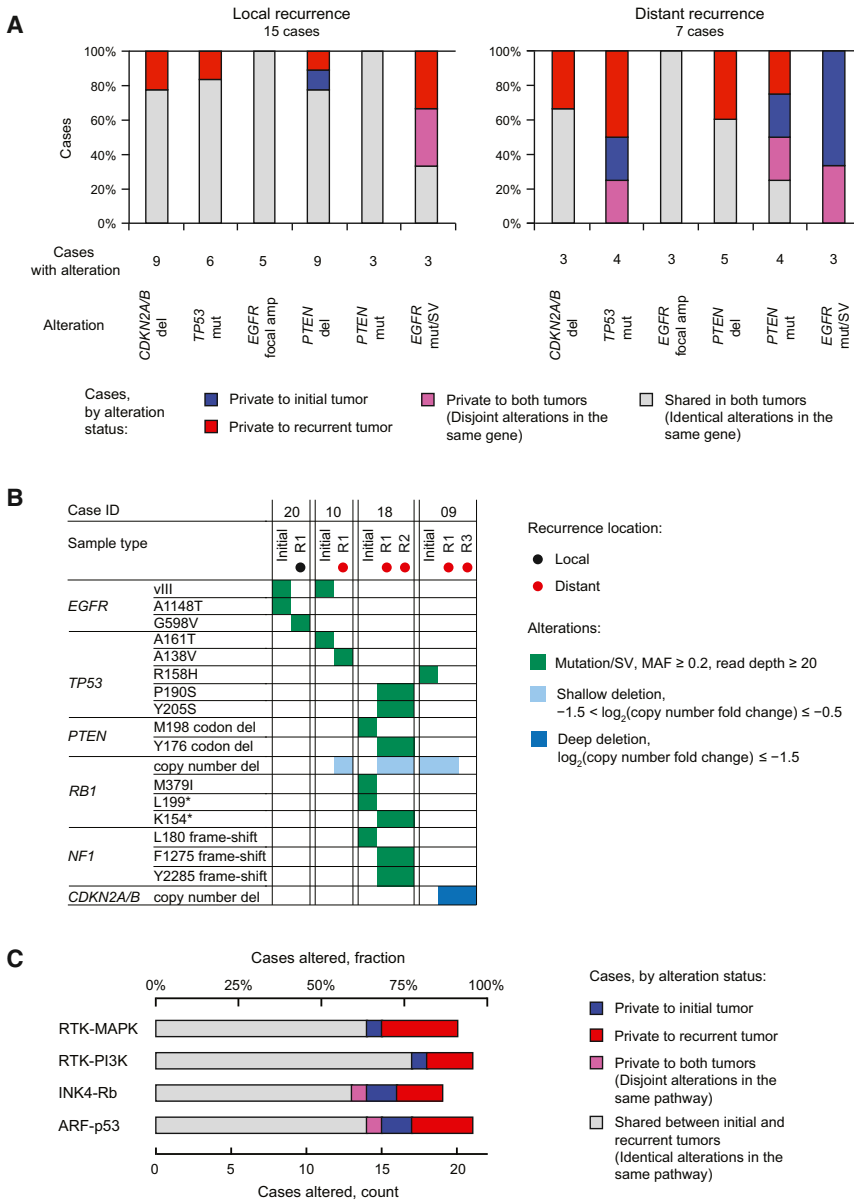


**Figure 3. Divergence and Convergence of Key GBM Driver Alterations at Recurrence**

(A) Private or shared presence of key GBM driver gene alterations in local and distance recurrence cases. Alterations detected in three or more cases of both local and distant recurrence groups were examined. The 22 cases with WES data available for both the tumor and normal tissues were considered. The following alterations were considered: point mutations and indels ( $MAF \geq 0.2$  and read depth  $\geq 20$ ) and copy number changes ( $\geq 1.5$  and  $\leq -0.5$  for focal, high-amplitude amplification and heterozygous/homozygous deletion, respectively;  $\log_2$  scale) detected in WES; structural variants (SVs;  $MAF \geq 0.2$  and read depth  $\geq 20$ ) detected in RNA-seq.

(B) Summary of changes in key genes/pathways in the four cases that show evidence of convergent evolution.

(C) Private or shared mutations in key GBM driver pathways. Cases and alterations that are considered for this analysis are as in (A).

See also [Figure S2](#) and [Table S5](#).

profiling studies, including the TCGA GBM study ([Cancer Genome Atlas Research Network, 2008](#)), identified deregulation of four major pathways: RTK-MAPK, RTK-PI3K, INK4-Rb, and ARF-p53 pathways. Consistent with this, we found the four pathways to be altered in a majority of our initial tumors: 68% for RTK-MAPK, 82% for RTK-PI3K, 73% for INK4-Rb, and 78% for ARF-p53 ([Figures 3C and S2B](#)). In our recurrent tumors, pathway alterations were detected even more frequently: 86% for RTK-MAPK, 91% for RTK-PI3K, 77% for INK4-Rb, and 86% for ARF-p53. In addition, the number of tumors that have alterations in all four pathways was increased in the recurrent tumor set: from 50% (11 of 22) of initial tumors to 73% (16 of 22) of recurrent tumors. These data are

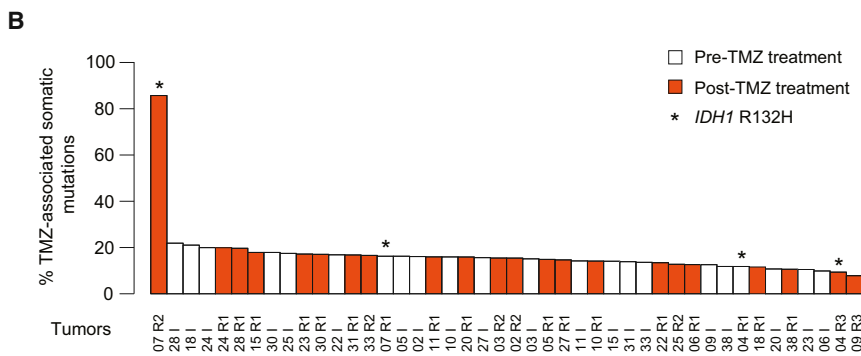
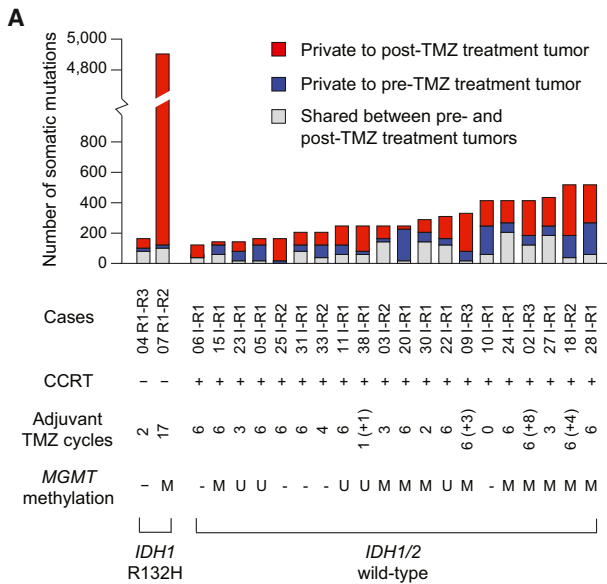
this patient did not have the above alterations but instead had homozygous deletion of *CDKN2A*. Therefore, both INK4-Rb and ARF-p53 pathways were dysregulated in both the initial and recurrent tumors but at different nodes of the pathway in each tumor. In sum, these results suggest that although the initial and recurrent tumors frequently branch out early and evolve independently, in some cases, they experience common selective pressure to acquire alterations in overlapping driver genes or pathways.

**Distinct Pathway Alteration Landscapes of Initial versus Recurrent Tumors**

Substantial difference in driver alterations between the initial and recurrent tumors suggests the possibility that recurrent tumors have a distinct landscape of oncogenic pathway alterations compared with initial tumors. Large-scale genomic

consistent with the notion that the recurrent tumors typically have more comprehensive and extensive alterations in major oncogenic pathways compared with their corresponding initial tumors.

We also performed unsupervised pathway analysis on the basis of the gene expression difference between the matched initial and recurrent tumors. Using gene set enrichment analysis ([Subramanian et al., 2005](#)), we found that gene sets that are significantly upregulated in recurrent tumors are predominantly neural and ion channel gene sets (65% and 13%, respectively;  $p < 0.001$  for both, after multiple hypothesis correction; [Figures S2C and S2D](#) and [Table S5](#)). This result is consistent with a published finding that infiltrating normal astrocytes protect brain-metastasized melanoma cells from chemotherapy by sequestering calcium away from the tumor cells through cell-to-cell gap junctions ([Lin et al., 2010](#)), suggesting a hypothesis



that normal neuronal cells in the tumor microenvironment contribute to GBM recurrence.

### Minimal TMZ-Induced Mutations in Primary GBMs

To determine the extent of mutations induced by TMZ, we systematically examined the number and characteristics of somatic mutations in our paired pre- and post-TMZ treatment GBM specimens. Consistent with the results of Johnson et al. (2014), the post-TMZ treatment tumor from an *IDH1*-R132H secondary GBM patient (case 07) in our cohort showed a dramatically increased number of somatic mutations compared with the matched TMZ-naïve tumor (4,858 versus 119; Figure 4A); this patient was treated only with TMZ between the two surgical procedures (Figure S1B). The recurrent tumor in this case had mutations in mismatch repair genes (*PMS1* and *MSH5*), as is typical for tumors with hypermutation (Hunter et al., 2006; Johnson et al., 2014). By mutation signature analysis (Alexandrov et al., 2013; Lawrence et al., 2013), we found that TMZ treatment was responsible for these mutations (Figures 4B and S3A–S3C). In sharp contrast, none of the 20 *IDH1*-wild-type primary GBM patients—all of whom received TMZ treatment (as part of concurrent chemoradiotherapy [CCRT] or/and adjuvant chemotherapy; Figure S1B)—showed any notable increase in the total or TMZ-associated mutations in the recurrent tumors compared

### Figure 4. Minimal TMZ-Induced Mutations in Primary GBMs

(A) The number of somatic mutations in the pre- and post-TMZ treatment tumors. For the cases with three available longitudinal tumors, the first and the last tumors were considered. Treatments administered between the first and last available resections were indicated; numbers in parentheses indicate TMZ cycles under the low-dose regimen. Case label and *MGMT* promoter methylation status are as in Figure 1. (B) Frequency of TMZ-associated somatic mutations in pre-TMZ treatment tumors versus post-TMZ treatment tumors. Tumors considered for this analysis are as in (A). See also Figure S3.

with the initial tumors (Figures 4A and 4B). Moreover, the signature of the recurrent tumor mutations was mostly unchanged from that of the corresponding initial tumors (Figure S3D). When we extended our hypermutation analysis to five additional cases in our cohort for which WES data were available for the tumors but not for the matched normal tissues (cases 01, 08, 14, 26, and 36), no evidence of hypermutation was detected in post-TMZ treatment tumors of these cases (Figure S3E). The lack of TMZ-associated hypermutation in our primary GBM specimens contrasts with the results from Johnson et al. (2014) and argues against the possibility of high risk of TMZ-induced hypermutation in primary GBMs. The difference between *IDH1*-mutated and *IDH1*-wild-type tumors can be potentially explained by multiple factors, including the differences in treatment regimen and *MGMT* promoter methylation (see Discussion; Figure S3F).

### DISCUSSION

Tumor evolution is a dynamic process both spatially and temporally, and it is often accelerated by therapeutic interventions such as chemotherapy and radiation. Understanding this evolutionary process would provide clues for guiding effective therapies. By integrative genomic analysis of the matched initial and recurrent tumors from patients with primary GBM, we obtained findings that have immediate clinical and biological implications. First, we found two paths of tumor evolution leading to GBM recurrence. Distally recurred tumors shared only a minority of initial tumor mutations, indicative of branched evolution (also called divergent evolution). In contrast, most of locally recurred tumors shared a majority of initial tumor mutations, consistent with linear evolution. At distant recurrence, genetic divergence between the initial and recurrent tumors entailed changes in key GBM driver gene/pathway alterations. Recent studies on paired gliomas (Johnson et al., 2014) and GBMs (Kim et al., 2015) also reported two types of genome evolution at recurrence, linear and



branched, on the basis of the extent of genetic similarity between the initial and recurrent tumors. With full radiographic data available for all our patients, we found that the pattern of genomic evolution can be predicted by the location of GBM recurrence with respect to the initial tumor.

Studies of the paired primary and metastatic tumors (Wu et al., 2012b; Yachida et al., 2010) and initial-relapsed leukemia (Ding et al., 2012; Walter et al., 2012) revealed substantial genomic divergence between the paired specimens, suggesting that clonal selection might be a major mechanism in metastasis and relapse. However, it has been unclear whether such clonal selection happens at GBM recurrence. Our results suggest that although GBMs recur within the brain, GBM recurrence at a distant location of the brain involves a high degree of clonal selection and consequent genomic divergence. For the mechanism of clonal selection at distant recurrence, we speculate that tumor clones that had diffusely invaded into the brain parenchyma at the early stage of tumor development may escape its dormant state and repopulate the recurrent tumor at distal locations, a hypothesis worthy of further examination.

Although a large number of clinical trials have been conducted for recurrent GBM patients who no longer tolerate or respond to the standard treatment, the treatment options considered in those trials are based on the genomic profiles of their naive tumors. Our finding that genomic profiles, including alterations of key drivers, of distant recurrent tumors are highly divergent from those of the initial tumors raises serious concern that the genomic profile of the initial tumor may mislead subsequent therapies. Our results suggest that re-biopsy and re-profiling may be essential for more accurate clinical decisions, at least for patients with distally recurred tumors.

Finally, our results indicated that in contrast to low-grade gliomas or secondary GBMs, primary GBMs rarely develop hypermutation following TMZ treatment. This dichotomy can be potentially explained by multiple factors, including differences in treatment regimen. Primary GBM patients in our cohort received CCRT (which includes radiation and ~1.5 cycles [6 weeks] of TMZ), followed by an additional 5.1 cycles of TMZ on average (median 6 cycles) as adjuvant therapy (counting 4 week-long regular or low-dose TMZ treatments as 1 cycle). The regimen is in accordance with the standard treatment protocol for primary GBM, which is CCRT followed by an additional 6 cycles of adjuvant TMZ (Stupp et al., 2005). In contrast, our secondary GBM patient (case 07) and the six low-grade glioma patients of Johnson et al. (2014) whose tumors developed hypermutation did not receive CCRT but received far more cycles (17 cycles for case 07 and 11.7 cycles on average for Johnson's six patients) of TMZ than did the primary GBM cohort. The higher total dose of TMZ and the fact that TMZ was administered outright without the preceding CCRT might have contributed to the higher incidence rate of hypermutation in the low-grade gliomas or secondary GBMs with *IDH1* mutation.

Another factor that may explain the difference in frequency of hypermutation is that *IDH1*-mutated tumors are predisposed to hypermutation by the following mechanism. The gain-of-function *IDH1* mutation at arginine 132 causes CpG island methylator phenotype, and as a result, the *IDH1*-mutated tumors show hypermethylation in a large fraction of the genome (Noushmehr et al., 2010; Turcan et al., 2012), frequently including the pro-

motor region of *MGMT*. The *MGMT* methylation and consequent *MGMT* silencing impairs a mechanism for repairing TMZ-induced DNA alkylation and mutagenesis (Liu and Gerson, 2006). Therefore, the *IDH1*-mutated tumors have a higher chance of acquiring inactivating mutations in mismatch repair genes and resulting hypermutation. Together, we hypothesize that genetic predisposition, in combination with the larger number of TMZ cycles administered to patients with *IDH1*-mutated tumors, accounts for the higher incidence rate of hypermutation in these tumors.

Irrespective of potential molecular mechanisms, our results provide important insights for clinical practice regarding GBM patients. TMZ-induced hypermutation and resulting large mutational diversity can contribute to drug resistance (Bozic et al., 2013); our data suggest that such an adverse effect of TMZ is minimal for *IDH1*-wild-type primary GBM patients when used in accordance with the standard regimen. On the other hand, for patients with *IDH1*-mutated tumors, who often show *MGMT* promoter methylation, TMZ has been considered a preferred treatment option and is often administered with more cycles than for other patients; this was based on the proven efficacy of TMZ for *MGMT*-methylated tumors (Hegi et al., 2005). However, on the basis of our study and the prior study on paired gliomas with *IDH1* mutations (Johnson et al., 2014), the benefits of TMZ should now be considered more carefully against its potentially adverse effects of hypermutation.

In summary, our systematic comparison of the genomic landscape of primary GBMs at initial diagnosis and recurrence provides one explanation for the ineffectiveness of targeted therapy for distally recurred tumors and illustrates the importance of re-biopsy and re-profiling for these tumors. Future studies with serial sampling of large cohorts will be needed to characterize genomic divergence of recurrent tumors in different tumor types and to measure potential side effects of existing therapies at the genomic level.

## EXPERIMENTAL PROCEDURES

### Patients and Specimens

This study was approved by the institutional review board at Samsung Medical Center and Seoul National University Hospital. Surgical specimens and clinical information were obtained from GBM patients who underwent brain tumor removal surgery at Samsung Medical Center and Seoul National University Hospital. Informed consent was obtained from all patients. All patients had well-annotated clinical information. On the basis of examination of preoperative MR images, the locations of recurrent tumors relative to initial tumors (local versus distant) were determined for all recurrent tumors. The presence of non-necrotic tumor regions in the specimens was confirmed through microscopic examination by trained pathologists. Histologic diagnoses of tumors were made by the pathologists. For genomic analysis, parts of the specimens were snap-frozen and preserved in liquid nitrogen until use. Genomic DNA and mRNA were extracted using the DNeasy kit and the RNeasy kit (Qiagen), respectively. WES, RNA-seq, and/or aCGH data were obtained for longitudinal specimens of 38 cases (i.e., longitudinal sampling panel). The study was designed to characterize how major GBM driver variants change in response to standard treatments rather than to discover rare variants. As such, the sample size of 38 cases (pairs or trios of tumors) provided >95% confidence for detecting (1) at least one case of any 10% frequency event (1 among 10 patients carries the variant) and (2) at least three cases of any 20% frequency event. The 38 cases were selection biased toward longer survival (median overall survival 27 versus 15 months in historical cohorts) and younger age (median age 47 versus 56 years in historical cohorts), because those patients are more likely

to have undergone more than one surgical procedure. In addition to the longitudinal sampling panel, we obtained WES data for 6 GBM cases, for which two geographically distinct specimens were obtained from a common untreated tumor (i.e., geographic sampling panel). We also used the TCGA data set; the analysis procedure for this data set is described in [Supplemental Experimental Procedures](#).

### aCGH

aCGH was conducted using Agilent SurePrint G3 Human CGH 4 × 180k arrays, according to the manufacturer's instructions. aCGH feature extraction files were processed and normalized using Agilent Genomic WorkBench 7.0.4.0 with the 022060\_20101001.xml design file (obtained from AgilentCytoGenomics 2.7.11.0). The R package DNACopy (version 1.30.0) was used to estimate DNA copy number for genomic segments. From the copy numbers at the segment level, the copy number for each gene was calculated by averaging the copy numbers of all exonic segments of the gene.

### WES

#### Raw Data

Either the Illumina TruSeq Exome-capture kit (for case 30) or the Agilent SureSelect kit (for all the other cases) was used for capturing exonic DNA fragments. For sequencing, Illumina HiSeq2000 was used to generate 2 × 101 bp paired-end reads.

#### Somatic Mutation

The sequenced reads in FASTQ files were mapped on the human genome assembly (hg19) using Burrows-Wheeler Aligner version 0.6.2 (Liu et al., 2009). The initial alignment BAM files were subjected to conventional preprocessing before mutation calling: sorting, removing duplicated reads, locally realigning reads around potential small indels, and recalibrating base quality scores using SAMtools, Picard version 1.73 and Genome Analysis ToolKit (GATK) version 2.5.2 (DePristo et al., 2011). dbSNP (build ID 135) was used in the realignment and recalibration processes. For mutation calling, MuTect (version 1.1.4) (Cibulskis et al., 2013) and SomaticIndelDetector (GATK version 2.2) (Banerji et al., 2012) were used to make high-confidence predictions on somatic mutations from the tumor and normal tissue pair. Variant Effect Predictor (VEP) version 73 (McLaren et al., 2010) was used to annotate the predicted somatic mutations with potential functional consequences and other relevant information. Procedures for coverage calculation, mutation calling for tumors without the available matched normal, mutation validation, and hypermutation status determination are described in [Supplemental Experimental Procedures](#).

#### Phylogeny

The evolutionary relationship between multiple tumors obtained from the same individual was inferred from the patterns of somatic mutations. We used Phylip version 3.695 to build phylogenetic trees. Only the mutations with read depth  $\geq 5$  in all related tumors of each case were used for this analysis.

#### Copy Number

We used the ngCGH python package version 0.4.4, which generates aCGH-like data from WES data. The patient-matched normal WES data were used as the reference for calculating fold changes in copy number in tumors. In cases in which patient-matched normal data were not available, we created a "pseudo-normal" profile to be used as the reference. The pseudo-normal profile is based on averaging a pool of 20 randomly chosen normal WES data, which were generated using the same sequencing platform and analysis pipeline as the tumor data. Downstream analyses, including segmentation and calculation of the copy number for each gene, were conducted as were done for aCGH data. For the tumors for which tumor purity was calculated, copy numbers were corrected for tumor purity as described in [Supplemental Experimental Procedures](#). For cases with both aCGH and WES data, the copy numbers measured from WES data were used for analysis.

#### RNA-seq

For all samples, RNA-seq libraries were prepared using the Illumina TruSeq RNA Sample Prep kit. RNA-seq data were analyzed for three types of information: mRNA level, exon skipping, and point mutation. For analysis of mRNA level, sequenced reads in FASTQ files were trimmed to include only 30 nucleotides from the 5' end of each read. The trimmed reads were mapped on hg19 using GSNAP version 2012-12-20 (Wu and Nacu, 2010), not allowing any

mismatch, indels, or splicing. The resulting alignment SAM files were sorted and summarized into BED files using SAMtools and bedTools (bamToBed version 2.16.2) (Quinlan and Hall, 2010). The BED files were used to calculate reads per kilobase of transcript per million reads mapped values for each gene by using the R package DEGseq (Wang et al., 2010) and the RefSeq gene annotations (refFlat table, downloaded from the University of California, Santa Cruz [UCSC] Genome Browser, last accessed on August 6, 2012). Procedures for unsupervised pathway analysis and subtype prediction (both analyses are based on mRNA level data) are described in [Supplemental Experimental Procedures](#). For analysis of exon skipping, the untrimmed reads in FASTQ files were aligned on hg19 using GSNAP in the single-end mapping mode, while allowing splicing. The GSNAP results were parsed to isolate the "split" reads that span non-canonical splicing junctions (not annotated in the RefSeq or UCSC Known Gene database), with the minimal anchor of five nucleotides on each exon. If there were more than two such split reads between two exons, the event was called as a skipped exon event between the two exons. For analysis of point mutations, full-length sequencing reads in FASTQ files were aligned on hg19 using GSNAP with the same configurations as for skipped exon detection (single-end mapping mode allowing splicing), except for the output format: skipped exon analysis used a GSNAP output, while point mutation analysis used a SAM-formatted output. The SAM files were subjected to the same preprocessing procedures as the ones applied to the WES data, except that local realignments were restricted to exonic regions, so as not to confuse normal splicing events as misaligned indels. We identified potential point mutations using UnifiedGenotyper of GATK and selected mutations that met the following criteria: (1) per-base sequencing depth  $\geq 4$ , (2) mutant allele read count  $\geq 2$ , (3) MAF  $\geq 0.01$ , and (4) chromosomal coordinate of a mutation is registered as "confirmed somatic mutation" in the COSMIC database. The selected mutation candidates were annotated using VEP as with WES data.

### ACCESSION NUMBERS

The raw and processed genomic data of this study have been deposited in the European Genome-Phenome Archive (WES and RNA-seq data; EGAS00001001041) and the Gene Expression Omnibus (GEO) (aCGH data; GEO: GSE63035).

### SUPPLEMENTAL INFORMATION

Supplemental Information includes Supplemental Experimental Procedures, three figures, and five tables and can be found with this article online at <http://dx.doi.org/10.1016/j.ccell.2015.07.013>.

### AUTHOR CONTRIBUTIONS

J.K., I.-H.L., and H.J.C. performed analyses. C.-K.P., D.-S.K., H.J.S., J.-I.L., and D.-H.N. provided specimens. Y.-S.J., Y.K., S.H.N., B.S.K., K.M.J., Y.Y., and W.-Y.P. organized and processed specimens. J.K., J.L., and P.J.P. wrote the manuscript, with feedback from I.-H.L., H.J.C., M.D.J., and D.-H.N. D.-H.N. designed the study and supervised the entire project.

### CONFLICTS OF INTEREST

J.K. is an employee of Samsung Electronics Co., Ltd.

### ACKNOWLEDGMENTS

We thank Yena Kim, Seahee Kim, and Hyun Ju Kang for technical assistance. This work was supported by the Korea Healthcare Technology R&D Project HI14C3418 (D.-H.N.) and HI13C2096 (W.-Y.P.) from the Korea Health Industry Development Institute and Ministry for Health & Welfare Affairs, Korea.

Received: November 7, 2014

Revised: June 10, 2015

Accepted: July 28, 2015

Published: September 14, 2015

## REFERENCES

- Alexandrov, L.B., Nik-Zainal, S., Wedge, D.C., Aparicio, S.A., Behjati, S., Biankin, A.V., Bignell, G.R., Bolli, N., Borg, A., Børresen-Dale, A.L., et al. (2013). Australian Pancreatic Cancer Genome Initiative; ICGC Breast Cancer Consortium; ICGC MMML-Seq Consortium; ICGC PedBrain (2013). Signatures of mutational processes in human cancer. *Nature* 500, 415–421.
- Banerji, S., Cibulskis, K., Rangel-Escareno, C., Brown, K.K., Carter, S.L., Frederick, A.M., Lawrence, M.S., Sivachenko, A.Y., Sougnez, C., Zou, L., et al. (2012). Sequence analysis of mutations and translocations across breast cancer subtypes. *Nature* 486, 405–409.
- Batra, S.K., Castelino-Prabhu, S., Wikstrand, C.J., Zhu, X., Humphrey, P.A., Friedman, H.S., and Bigner, D.D. (1995). Epidermal growth factor ligand-independent, unregulated, cell-transforming potential of a naturally occurring human mutant EGFRvIII gene. *Cell Growth Differ.* 6, 1251–1259.
- Bodell, W.J., Gaikwad, N.W., Miller, D., and Berger, M.S. (2003). Formation of DNA adducts and induction of lacI mutations in Big Blue Rat-2 cells treated with temozolomide: implications for the treatment of low-grade adult and pediatric brain tumors. *Cancer Epidemiol. Biomarkers Prev.* 12, 545–551.
- Bozic, I., Reiter, J.G., Allen, B., Antal, T., Chatterjee, K., Shah, P., Moon, Y.S., Yaquibie, A., Kelly, N., Le, D.T., et al. (2013). Evolutionary dynamics of cancer in response to targeted combination therapy. *eLife* 2, e00747.
- Brennan, C.W., Verhaak, R.G., McKenna, A., Campos, B., Nounshmehr, H., Salama, S.R., Zheng, S., Chakravarty, D., Sanborn, J.Z., Berman, S.H., et al.; TCGA Research Network (2013). The somatic genomic landscape of glioblastoma. *Cell* 155, 462–477.
- Cahill, D.P., Levine, K.K., Betensky, R.A., Codd, P.J., Romany, C.A., Reavie, L.B., Batchelor, T.T., Futreal, P.A., Stratton, M.R., Curry, W.T., et al. (2007). Loss of the mismatch repair protein MSH6 in human glioblastomas is associated with tumor progression during temozolomide treatment. *Clin. Cancer Res. an official journal of the American Association for Cancer Research* 13, 2038–2045.
- Cancer Genome Atlas Research Network (2008). Comprehensive genomic characterization defines human glioblastoma genes and core pathways. *Nature* 455, 1061–1068.
- Cibulskis, K., Lawrence, M.S., Carter, S.L., Sivachenko, A., Jaffe, D., Sougnez, C., Gabriel, S., Meyerson, M., Lander, E.S., and Getz, G. (2013). Sensitive detection of somatic point mutations in impure and heterogeneous cancer samples. *Nat. Biotechnol.* 31, 213–219.
- Cuddapah, V.A., Robel, S., Watkins, S., and Sontheimer, H. (2014). A neurocentric perspective on glioma invasion. *Nat. Rev. Neurosci.* 15, 455–465.
- DePristo, M.A., Banks, E., Poplin, R., Garimella, K.V., Maguire, J.R., Hartl, C., Philippakis, A.A., del Angel, G., Rivas, M.A., Hanna, M., et al. (2011). A framework for variation discovery and genotyping using next-generation DNA sequencing data. *Nat. Genet.* 43, 491–498.
- Ding, L., Ley, T.J., Larson, D.E., Miller, C.A., Koboldt, D.C., Welch, J.S., Ritchey, J.K., Young, M.A., Lamprecht, T., McLellan, M.D., et al. (2012). Clonal evolution in relapsed acute myeloid leukaemia revealed by whole-genome sequencing. *Nature* 481, 506–510.
- Esteller, M., Garcia-Foncillas, J., Andion, E., Goodman, S.N., Hidalgo, O.F., Vanaclocha, V., Baylin, S.B., and Herman, J.G. (2000). Inactivation of the DNA-repair gene MGMT and the clinical response of gliomas to alkylating agents. *N. Engl. J. Med.* 343, 1350–1354.
- Francis, J.M., Zhang, C.Z., Maire, C.L., Jung, J., Manzo, V.E., Adalsteinsson, V.A., Homer, H., Haidar, S., Blumenstiel, B., Pedamallu, C.S., et al. (2014). EGFR variant heterogeneity in glioblastoma resolved through single-nucleus sequencing. *Cancer Discov.* 4, 956–971.
- Furnari, F.B., Fenton, T., Bachoo, R.M., Mukasa, A., Stommel, J.M., Stegh, A., Hahn, W.C., Ligon, K.L., Louis, D.N., Brennan, C., et al. (2007). Malignant astrocytic glioma: genetics, biology, and paths to treatment. *Genes Dev.* 21, 2683–2710.
- Hegi, M.E., Diserens, A.C., Gorlia, T., Hamou, M.F., de Tribolet, N., Weller, M., Kros, J.M., Hainfellner, J.A., Mason, W., Mariani, L., et al. (2005). MGMT gene silencing and benefit from temozolomide in glioblastoma. *N. Engl. J. Med.* 352, 997–1003.
- Holland, E.C. (2000). Glioblastoma multiforme: the terminator. *Proc. Natl. Acad. Sci. USA* 97, 6242–6244.
- Hunter, C., Smith, R., Cahill, D.P., Stephens, P., Stevens, C., Teague, J., Greenman, C., Edkins, S., Bignell, G., Davies, H., et al. (2006). A hypermutation phenotype and somatic MSH6 mutations in recurrent human malignant gliomas after alkylator chemotherapy. *Cancer Res.* 66, 3987–3991.
- Jiao, Y., Killela, P.J., Reitman, Z.J., Rasheed, A.B., Heaphy, C.M., de Wilde, R.F., Rodriguez, F.J., Rosenberg, S., Oba-Shinjo, S.M., Nagahashi Marie, S.K., et al. (2012). Frequent ATRX, CIC, FUBP1 and IDH1 mutations refine the classification of malignant gliomas. *Oncotarget* 3, 709–722.
- Johnson, B.E., Mazor, T., Hong, C., Barnes, M., Aihara, K., McLean, C.Y., Fouse, S.D., Yamamoto, S., Ueda, H., Tatsuno, K., et al. (2014). Mutational analysis reveals the origin and therapy-driven evolution of recurrent glioma. *Science* 343, 189–193.
- Killela, P.J., Reitman, Z.J., Jiao, Y., Bettgowda, C., Agrawal, N., Diaz, L.A., Jr., Friedman, A.H., Friedman, H., Gallia, G.L., Giovannella, B.C., et al. (2013). TERT promoter mutations occur frequently in gliomas and a subset of tumors derived from cells with low rates of self-renewal. *Proc. Natl. Acad. Sci. USA* 110, 6021–6026.
- Kim, H., Zheng, S., Amini, S.S., Virk, S.M., Mikkelsen, T., Brat, D.J., Grimsby, J., Sougnez, C., Muller, F., Hu, J., et al. (2015). Whole-genome and multisector exome sequencing of primary and post-treatment glioblastoma reveals patterns of tumor evolution. *Genome Res.* 25, 316–327.
- Lawrence, M.S., Stojanov, P., Polak, P., Kryukov, G.V., Cibulskis, K., Sivachenko, A., Carter, S.L., Stewart, C., Mermel, C.H., Roberts, S.A., et al. (2013). Mutational heterogeneity in cancer and the search for new cancer-associated genes. *Nature* 499, 214–218.
- Lee, J.C., Vivanco, I., Beroukhi, R., Huang, J.H., Feng, W.L., DeBiasi, R.M., Yoshimoto, K., King, J.C., Nghiemphu, P., Yuza, Y., et al. (2006). Epidermal growth factor receptor activation in glioblastoma through novel missense mutations in the extracellular domain. *PLoS Med.* 3, e485.
- Lin, Q., Balasubramanian, K., Fan, D., Kim, S.J., Guo, L., Wang, H., Bar-Eli, M., Aldape, K.D., and Fidler, I.J. (2010). Reactive astrocytes protect melanoma cells from chemotherapy by sequestering intracellular calcium through gap junction communication channels. *Neoplasia* 12, 748–754.
- Liu, L., and Gerson, S.L. (2006). Targeted modulation of MGMT: clinical implications. *Clin. Cancer Res. an official journal of the American Association for Cancer Research* 12, 328–331.
- Liu, Q., Nguyen, D.H., Dong, Q., Shitaku, P., Chung, K., Liu, O.Y., Tso, J.L., Liu, J.Y., Konkankit, V., Cloughesy, T.F., et al. (2009). Molecular properties of CD133+ glioblastoma stem cells derived from treatment-refractory recurrent brain tumors. *J. Neurooncol.* 94, 1–19.
- McLaren, W., Pritchard, B., Rios, D., Chen, Y., Flicek, P., and Cunningham, F. (2010). Deriving the consequences of genomic variants with the Ensembl API and SNP Effect Predictor. *Bioinformatics* 26, 2069–2070.
- Nathanson, D.A., Gini, B., Mottahedeh, J., Visnyei, K., Koga, T., Gomez, G., Eskin, A., Hwang, K., Wang, J., Masui, K., et al. (2014). Targeted therapy resistance mediated by dynamic regulation of extrachromosomal mutant EGFR DNA. *Science* 343, 72–76.
- Nounshmehr, H., Weisenberger, D.J., Diefes, K., Phillips, H.S., Pujara, K., Berman, B.P., Pan, F., Pelloski, C.E., Sulman, E.P., Bhat, K.P., et al.; Cancer Genome Atlas Research Network (2010). Identification of a CpG island methylator phenotype that defines a distinct subgroup of glioma. *Cancer Cell* 17, 510–522.
- Parsons, D.W., Jones, S., Zhang, X., Lin, J.C., Leary, R.J., Angenendt, P., Mankoo, P., Carter, H., Siu, I.M., Gallia, G.L., et al. (2008). An integrated genomic analysis of human glioblastoma multiforme. *Science* 321, 1807–1812.
- Patel, A.P., Tirosh, I., Trombetta, J.J., Shalek, A.K., Gillespie, S.M., Wakimoto, H., Cahill, D.P., Nahed, B.V., Curry, W.T., Martuza, R.L., et al. (2014). Single-cell RNA-seq highlights intratumoral heterogeneity in primary glioblastoma. *Science* 344, 1396–1401.
- Quinlan, A.R., and Hall, I.M. (2010). BEDTools: a flexible suite of utilities for comparing genomic features. *Bioinformatics* 26, 841–842.

- Schwartzentruber, J., Korshunov, A., Liu, X.Y., Jones, D.T., Pfaff, E., Jacob, K., Sturm, D., Fontebasso, A.M., Quang, D.A., Tönjes, M., et al. (2012). Driver mutations in histone H3.3 and chromatin remodelling genes in paediatric glioblastoma. *Nature* **482**, 226–231.
- Snuderl, M., Faziollahi, L., Le, L.P., Nitta, M., Zhelyazkova, B.H., Davidson, C.J., Akhavanfard, S., Cahill, D.P., Aldape, K.D., Betensky, R.A., et al. (2011). Mosaic amplification of multiple receptor tyrosine kinase genes in glioblastoma. *Cancer Cell* **20**, 810–817.
- Sottoriva, A., Spiteri, I., Piccirillo, S.G., Touloumis, A., Collins, V.P., Marioni, J.C., Curtis, C., Watts, C., and Tavaré, S. (2013). Intratumor heterogeneity in human glioblastoma reflects cancer evolutionary dynamics. *Proc. Natl. Acad. Sci. USA* **110**, 4009–4014.
- Stevens, M.F., and Newlands, E.S. (1993). From triazines and triazines to temozolomide. *Eur. J. Cancer* **29A**, 1045–1047.
- Stupp, R., Mason, W.P., van den Bent, M.J., Weller, M., Fisher, B., Taphoorn, M.J., Belanger, K., Brandes, A.A., Marosi, C., Bogdahn, U., et al.; European Organisation for Research and Treatment of Cancer Brain Tumor and Radiotherapy Groups; National Cancer Institute of Canada Clinical Trials Group (2005). Radiotherapy plus concomitant and adjuvant temozolomide for glioblastoma. *N. Engl. J. Med.* **352**, 987–996.
- Stupp, R., Hegi, M.E., Gilbert, M.R., and Chakravarti, A. (2007). Chemoradiotherapy in malignant glioma: standard of care and future directions. *J. Clin. Oncol.* **25**, 4127–4136.
- Sturm, D., Witt, H., Hovestadt, V., Khuong-Quang, D.A., Jones, D.T., Konermann, C., Pfaff, E., Tönjes, M., Sill, M., Bender, S., et al. (2012). Hotspot mutations in H3F3A and IDH1 define distinct epigenetic and biological subgroups of glioblastoma. *Cancer Cell* **22**, 425–437.
- Subramanian, A., Tamayo, P., Mootha, V.K., Mukherjee, S., Ebert, B.L., Gillette, M.A., Paulovich, A., Pomeroy, S.L., Golub, T.R., Lander, E.S., and Mesirov, J.P. (2005). Gene set enrichment analysis: a knowledge-based approach for interpreting genome-wide expression profiles. *Proc. Natl. Acad. Sci. USA* **102**, 15545–15550.
- Sugawa, N., Ekstrand, A.J., James, C.D., and Collins, V.P. (1990). Identical splicing of aberrant epidermal growth factor receptor transcripts from amplified rearranged genes in human glioblastomas. *Proc. Natl. Acad. Sci. USA* **87**, 8602–8606.
- Tanaka, S., Louis, D.N., Curry, W.T., Batchelor, T.T., and Dietrich, J. (2013). Diagnostic and therapeutic avenues for glioblastoma: no longer a dead end? *Nat. Rev. Clin. Oncol.* **10**, 14–26.
- Turcan, S., Rohle, D., Goenka, A., Walsh, L.A., Fang, F., Yilmaz, E., Campos, C., Fabius, A.W., Lu, C., Ward, P.S., et al. (2012). IDH1 mutation is sufficient to establish the glioma hypermethylator phenotype. *Nature* **483**, 479–483.
- Verhaak, R.G., Hoadley, K.A., Purdom, E., Wang, V., Qi, Y., Wilkerson, M.D., Miller, C.R., Ding, L., Golub, T., Mesirov, J.P., et al.; Cancer Genome Atlas Research Network (2010). Integrated genomic analysis identifies clinically relevant subtypes of glioblastoma characterized by abnormalities in PDGFRA, IDH1, EGFR, and NF1. *Cancer Cell* **17**, 98–110.
- Walter, M.J., Shen, D., Ding, L., Shao, J., Koboldt, D.C., Chen, K., Larson, D.E., McLellan, M.D., Dooling, D., Abbott, R., et al. (2012). Clonal architecture of secondary acute myeloid leukemia. *N. Engl. J. Med.* **366**, 1090–1098.
- Wang, L., Feng, Z., Wang, X., Wang, X., and Zhang, X. (2010). DESeq: an R package for identifying differentially expressed genes from RNA-seq data. *Bioinformatics* **26**, 136–138.
- Wu, T.D., and Nacu, S. (2010). Fast and SNP-tolerant detection of complex variants and splicing in short reads. *Bioinformatics* **26**, 873–881.
- Wu, G., Broniscer, A., McEachron, T.A., Lu, C., Paugh, B.S., Becksfors, J., Qu, C., Ding, L., Huether, R., Parker, M., et al.; St. Jude Children's Research Hospital–Washington University Pediatric Cancer Genome Project (2012a). Somatic histone H3 alterations in pediatric diffuse intrinsic pontine gliomas and non-brainstem glioblastomas. *Nat. Genet.* **44**, 251–253.
- Wu, X., Northcott, P.A., Dubuc, A., Dupuy, A.J., Shih, D.J., Witt, H., Croul, S., Bouffet, E., Fults, D.W., Eberhart, C.G., et al. (2012b). Clonal selection drives genetic divergence of metastatic medulloblastoma. *Nature* **482**, 529–533.
- Yachida, S., Jones, S., Bozic, I., Antal, T., Leary, R., Fu, B., Kamiyama, M., Hruban, R.H., Eshleman, J.R., Nowak, M.A., et al. (2010). Distant metastasis occurs late during the genetic evolution of pancreatic cancer. *Nature* **467**, 1114–1117.
- Yan, H., Parsons, D.W., Jin, G., McLendon, R., Rasheed, B.A., Yuan, W., Kos, I., Batinic-Haberle, I., Jones, S., Riggins, G.J., et al. (2009). IDH1 and IDH2 mutations in gliomas. *N. Engl. J. Med.* **360**, 765–773.
- Yip, S., Miao, J., Cahill, D.P., Iafrate, A.J., Aldape, K., Nutt, C.L., and Louis, D.N. (2009). MSH6 mutations arise in glioblastomas during temozolomide therapy and mediate temozolomide resistance. *Clin. Cancer Res. an official journal of the American Association for Cancer Research* **15**, 4622–4629.